Journal of Solid State Chemistry **147,** 45–57 (1999)
Article ID jssc.1999.8152, available online at http://www.idealibrary.com on IDEAL®

Synthesis, Average Structure, and Magnetic Properties of Oxygen Deficient Perovskites $(Ba_{2-3x}Bi_{3x-1})(Fe_{2x}Bi_{1-2x})O_{2+3/2x}$

Ph. Boullay, M. Hervieu,[1] N. Nguyen, and B. Raveau

Laboratoire CRISMAT, UMR 6508, Université de Caen, 6, Bld du maréchal Juin, 14050 Caen Cedex, France

Received September 24, 1998; in revised form December 10, 1998; accepted December 20, 1998

THIS PAPER IS DEDICATED IN PROFESSOR JEAN ROUXEL'S MEMORY

A new family of oxygen deficient perovskite $[Ba_{2-3x}Bi_{3x-1}][Fe_{2x}Bi_{1-2x}]O_{2+3x/2}$ has been synthesized for $1/3 \leq x \leq 1/2$. The average structure of these phases is determined using a combination of X-ray, neutron powder diffraction, and electron diffraction. The compounds exhibit a cubic subcell ($a = a_p$) for $x \leq 0.43$ and a tetragonal subcell ($a \approx c \approx a_p$) for $0.43 < x \leq 0.50$. In fact, incommensurate satellite spots are observed for $0.40 \leq x \leq 0.50$, with a q=γc* vector varying regularly from $\gamma = 0.3$ for $x = 0.40$ to $\gamma = 0.25$ for $x = 0.50$. The distribution of Bi(III) between the two A and B sites is demonstrated. The Mössbauer study shows that iron is in the trivalent state and a progressive evolution of its coordination in the incommensurate samples. Magnetic susceptibility measurements evidence a magnetic transition for $x \geq 0.45$ samples, whose temperature T spreads from 620 to 720 K. The examination of the paramagnetic domain confirms that iron is trivalent with a high spin configuration ($\mu = 5\mu_B/Fe^{3+}$). The $M(H)$ curve registered at 5 K for $x = 0.50$ shows that this phase is a weak ferromagnet. The magnetic transition is confirmed by calorimetric measurements.

INTRODUCTION

The perovskite-type materials are known for their great variety of physical, chemical, or catalytic properties (1). However, in spite of the apparent simplicity of the "basic" perovskite structure, the relationships between their properties and the structure are not straightforward. In the last decade, the superconducting properties of perovskite-related compounds $Ba(Bi_{1-x}Pb_x)O_3$ (2), $(Ba_{1-x}K_x)BiO_3$ (3), or copper-based oxides (4)) and the colossal magnetoresistive properties of the manganese based oxides (5) have attracted much interest and illustrate this complexity. From the chemical and structural point of view, the factors governing the ordering of cations on the B site have been the object of a lot of work in complex perovskites $A(BB')O_3$, $(AA')(BB')O_3$, and oxygen deficient perovskites (see Refs. (1), (6), and (7) for a nonexhaustive review).

In a general way, much remains to be discovered about the magnetic and transport properties of transition metal oxides with the perovskite structures, taking into consideration the electron configuration of the transition element, its valence, but also the size of the A site cation, and the oxygen stoichiometry. In this respect, the system Ba–Bi––Fe–O, studied more than twenty years ago by Zanne *et al.* (8), is of great interest. Working with an oxygen pressure of 200 bars, these authors synthesized a series of perovskites $[Ba_{1-x}Bi_x][Fe_{1-x}Bi_x]O_{3-y}$, in which bismuth is distributed between the two A and B sites. Moreover, from the study of the magnetic and transport properties, they showed that both Fe and Bi exhibit a mixed valence, Fe(IV)/Fe(III) and Bi(III)/(Bi(V), respectively.

If one considers the possibility of a large oxygen deficiency in iron–bismuth perovskite, one may raise the question of the existence of Bi(III)–Fe(III) perovskites in the system Ba–Bi–Fe–O. For this reason we have reinvestigated this system, using a much lower oxygen pressure, i.e. working in air. In the present paper we report on the synthesis, average structure and magnetic properties of a new series of perovskites $[Ba_{2-3x}Bi_{3x-1}][Fe_{2x}Bi_{1-2x}]O_{2+3x/2}$ with $1/3 \leq x \leq 1/2$.

SYNTHESIS AND CHEMICAL COMPOSITION

The compounds $(Ba_{2-3x}Bi_{3x-1})(Fe_{2x}Bi_{1-2x})O_{2+3x/2}$ were prepared by solid state reaction of the appropriate ratio of $BaCO_3$, Bi_2O_3 and Fe_2O_3. The reagents were ground in an agate mortar and fired in alumina crucibles at 850°C in air for 1 day. The temperature was slowly decreased to room temperature at the rate of 50°C/hr. For powder neutron diffraction (PND) study, carried out on the terms $x > 0.40$, about 10–15 g of each starting powder was mechanically ground during 24 hr. The thermal treatment above was then applied two times with intermediate grinding.

[1] To whom correspondence should be addressed.

0022-4596/99 $30.00

The X-ray powder diffraction (XRPD) data, for the members $x \leq 0.43$, were recorded using a Philips PW3570 diffractometer with a nickel filtered CuK radiation. A 2θ scan, with a constant step width (0.02°) and a constant time count per step (10 s), was used to collect the data. The Rietveld structure analysis was performed with the program Fullprof (9). For the members $x > 0.43$, the data scan was optimized by using a nonconstant step width (smaller at low angles, larger at high angles) and a variable time count per step (shorter at low angles, longer at high angles). Further details about this recording will be given in a next paper (11). In this case, the Rietveld structure analysis was performed with the program XND (12)

NPD data were collected at room temperature in the range 0–160° on the high resolution powder diffractometer D1A (ILL Grenoble) using a wavelength = 1.909 Å.

The XRPD patterns (Fig. 1) show that single-phase materials are synthesized for $0.40 \leq x \leq 0.50$, whereas a minority phase, cubic $BaBiO_3$ (reference no. 38-1151 of the powder diffraction file), is observed for $0.33 \leq x < 0.40$.

The solid solution $(Ba_{2-3x}Bi_{3x-1})(Fe_{2x}Bi_{1-2x})O_{2+3x/2}$ was studied for $0.33 \leq x \leq 0.50$ using electron microscopy. The crystallites were crushed in alcohol and the small flakes deposited on holey carbon films, supported by a copper grid. The electron diffraction (ED) study was carried out with a JEOL 200CX (tilt $\pm$ 60°) electron microscope, reconstructing the reciprocal space by tilting around the different crystallographic axes.

The microscope is equipped with an energy dispersive spectroscopy (EDS) analyser and, for each sample, EDS analyses were performed on about 20 grains. A slight difference has been systematically observed between the nominal and actual compositions. The nominal and actual compositions are compared in Table 1 and the distribution of the cations is calculated on the basis of fully occupied cation sites. These differences can be considered as in the limit of the error for $0.40 < x \leq 0.50$, whereas they are significant for $0.33 \leq x \leq 0.40$, showing an iron excess with respect to the nominal content in agreement with the detection of $BaBiO_3$ as secondary phase. Several annealings were carried out in order to achieve the stabilization of $BaBiO_3$-free samples. All these attempts failed. Nevertheless, more drastic variations of the synthesis conditions were not considered since, as mentioned above, they may modify the Bi and Fe oxidation states.

The oxygen content was determined by redox titration (10). About 100 mg of the sample was dissolved in an excess of aqueous solution of $FeCl_2 \cdot 4H_2O$ (0.1 N), in presence of HCl (2 N) and H_3PO_4 (1 N). The ferrous ion reduces the Bi^{5+} to Bi^{3+} and the Fe^{4+} to Fe^{3+}. The excess of ferrous ion is then titrated by a solution of $K_2Cr_2O_7$ (0.1 N) in presence of a chemical indicator, $Ba(C_6H_5–NH–C_6H_4–SO_3)_2$. Assuming that the cationic content is given by EDS analyses, we are able to demonstrate the presence of Fe^{4+} or Bi^{5+} and then to have a good estimation of the oxygen content of the sample.

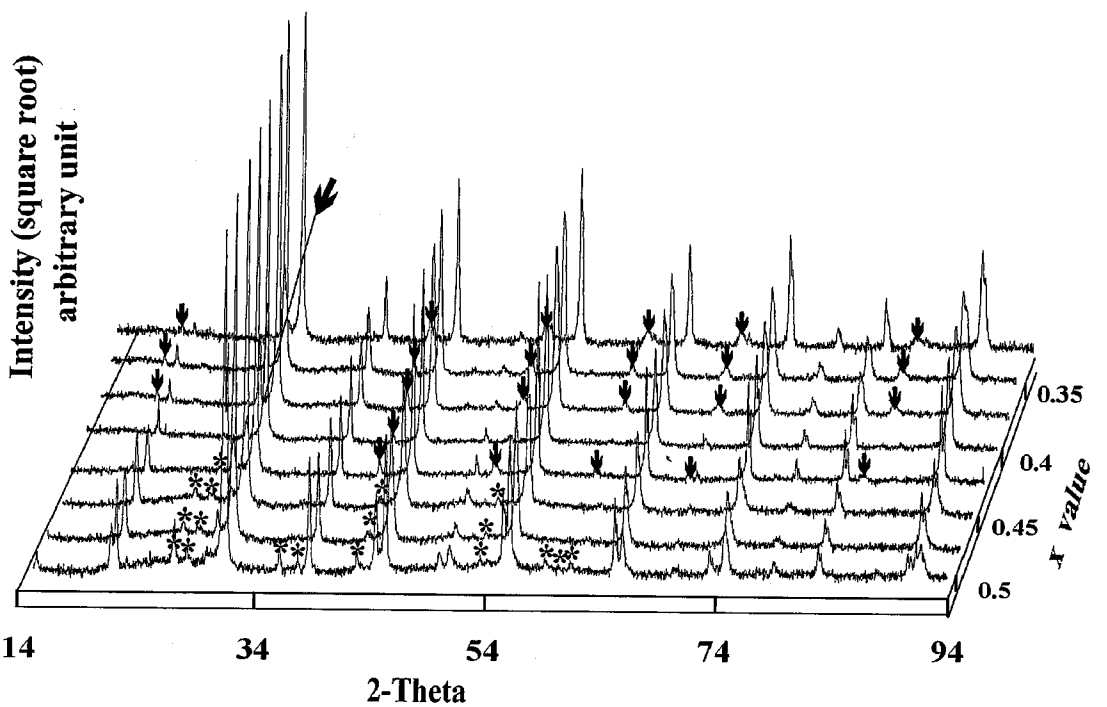

FIG. 1. Evolution of the XRPD patterns as a function of x (arrows indicate the reflections of the secondary $BaBiO_{3-\delta}$ phase, and stars, the weak satellites due to the modulated structure).

TABLE 1
Nominal and Actual Compositions of the Samples (from EDS Results)

Nominal cationic	x value	Actual cation content	Calculated distribution
$Ba_1\,Bi_{0.33}\,Fe_{0.67}$	0.33	$Ba_{0.94}\,Bi_{0.32}\,Fe_{0.74}$	$[Ba_{0.94}Bi_{0.06}]\,[Fe_{0.74}\,Bi_{0.26}]$
$Ba_{0.8}\,Bi_{0.4}\,Fe_{0.8}$	0.40	$Ba_{0.77}\,Bi_{0.38}\,Fe_{0.85}$	$[Ba_{0.77}Bi_{0.23}]\,[Fe_{0.85}\,Bi_{0.15}]$
$Ba_{0.65}\,Bi_{0.45}\,Fe_{0.9}$	0.45	$Ba_{0.63}\,Bi_{0.44}\,Fe_{0.93}$	$[Ba_{0.63}Bi_{0.37}]\,[Fe_{0.93}\,Bi_{0.07}]$
$Ba_{0.5}\,Bi_{0.5}\,Fe_1$	0.5	$Ba_{0.48}\,Bi_{0.52}\,Fe_1$	$[Ba_{0.48}Bi_{0.52}]\,[Fe_1]$

Due to the presence of $BaBiO_3$ as an impurity, the oxygen content of the $0.33 \leq x \leq 0.40$ samples were not analyzed. The chemical analyses of all the compounds corresponding to $0.40 \leq x \leq 0.50$ showed that there is no significant excess of oxygen with respect to the formula "$O_{2+3x/2}$," implying that bismuth and iron are both in the trivalent state. Note that in the present paper the formula always refer to the nominal composition using the x value of the ideal formula $[Ba_{2-3x}Bi_{3x-1}][Fe_{2x}Bi_{1-2x}]O_{2+3x/2}$.

CELL PARAMETERS

All the intense lines of the XRPD patterns can be indexed in a cubic cell with $a \approx a_p$ for $0.33 \leq x \leq 0.43$ and in a tetragonal cell ($a \approx c \approx a_p$) for $0.43 < x \leq 0.50$. The evolution of the cell parameters versus x (Fig. 2) shows that a decreases as x increases in both domains, cubic and tetragonal, whereas c increases in the tetragonal phase. In both domains, the cell volume decreases as x increases, in agreement with the decrease of the Bi(III) content in the B site and with its increase in the A site. Note that a set of weak extra reflections is observed for the tetragonal phase, i.e. for $0.43 < x \leq 0.50$. These additional reflections are not in commensurate positions referring to the perovskite subcell. They can be indexed using a modulation vector in the form $\mathbf{q} = \gamma\mathbf{c}^*$ and considered as satellite reflections. The γ value as well as the intensity of satellites vary with x. In Fig. 1, the intense satellite reflections are indicated by asterisks, the most intense one being $101\bar{1}$ (intereticular distance close to 3.25 Å). For the $x \geq 0.43$ members, only the satellite reflectins were not taken in account in the XRPD patterns used for the Rietveld refinement (see next section and Figs. 5 and 6).

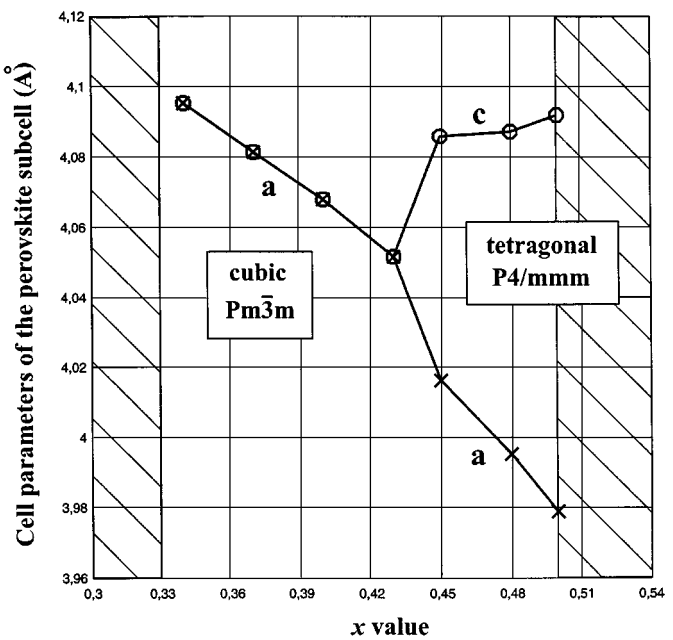

FIG. 2. Evolution of the perovskite cell parameters with x.

The [100] electron patterns recorded for different x values (Fig. 3) clearly confirm the existence of satellite reflections in incommensurate positions. They are observed by ED for all the $x \geq 0.4$ samples.

For $x = 0.33$, the reconstitution of the reciprocal space shows that the actual cell is cubic with $a = 4.09$ Å. It is the only sample which does not exhibit extra reflections. There is no condition limiting the reflection and we will retain the usual space group $Pm3m$ for the cubic perovskite structure. This suggests that, for the member $Ba[Bi_{0.33}Fe_{0.67}]O_{2.5}$, there is no long range ordering between Bi and Fe located in the B site (as well as between O and vacancy on the anionic site).

For $x = 0.35$, very weak extra reflections are observed (see the $[1\bar{1}0]$ ED patterns in Fig. 4a) which induce a cubic supercell with $a = 2a_p = 8.16$ Å and a F-type lattice centring. The existence of such a superstructure shows that an ordering phenomenon (presumably between Bi and Fe on the B site) occurs for the latter compound but, regarding the chemical composition $[Ba_{0.95}Bi_{0.05}][Fe_{0.7}Bi_{0.30}]O_{2.525}$, a statistical distribution of Bi and Fe still necessarily exists, at least over one of the two B sites. However, the weakness of the extra reflections suggests that this ordering is not prefectly established.

For $x = 0.40$, very weak extra reflections are also observed but they are at incommensurate positions. As an illustration, the [100] ED pattern is given in Fig. 3b and the difference between the member $x = 0.35$ and $x = 0.40$ is clearly observed in the $[1\bar{1}0]$ ED patterns in Fig. 4a and 4b,

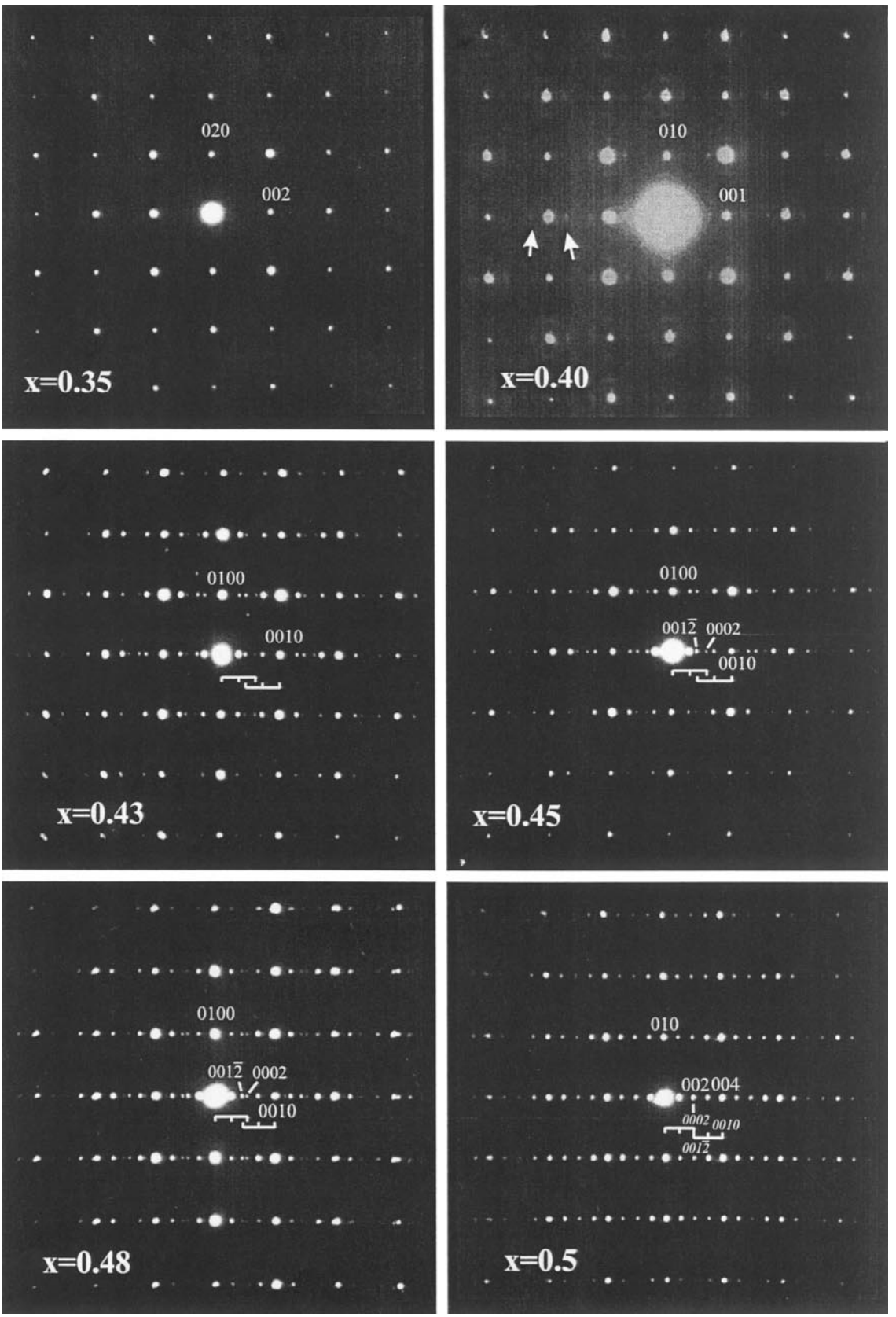

FIG. 3. [100] ED patterns recorded for different x values (the satellites are indexed using four *hklm* indices, the modulation vector is $\mathbf{q} = \gamma\mathbf{c}^*$).

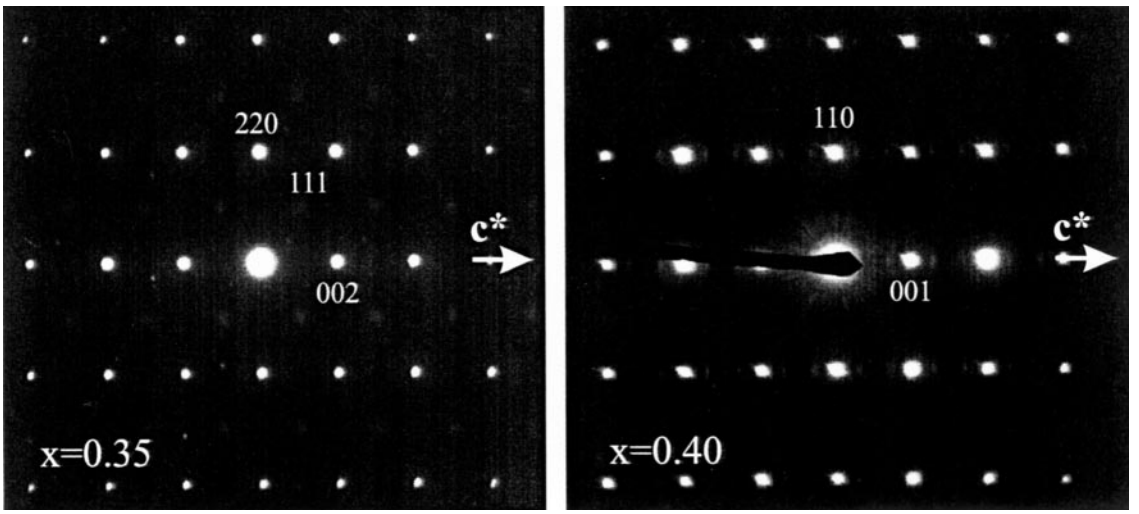

FIG. 4. [$1\bar{1}0$] ED patterns of the $x = 0.35$ and $x = 0.40$ samples.

respectively. For the composition $x = 0.40$, only the first order satellites are observed. Although the XRPD patterns indicate that this member is cubic,[2] the existence of satellite reflections along one particular direction implies that the actual symmetry is tetragonal with $a \approx c \approx a_p$ and $\mathbf{q} \approx 0.3\mathbf{c}^*$.

For the members $x = 0.43$, 0.45, and 0.48 (see the [100] ED patterns in Fig. 3c, d, and e, respectively), the intensity of the satellites increases with x and higher order satellites are observed up to the third order for the last two members). The value of the modulation vector $\mathbf{q} = \gamma\mathbf{c}^*$ regularly decreases as x increases, from 0.3 for the member $x = 0.40$ to 0.25 for the member $x = 0.50$. For this last member, the value is commensurate, which implies the existence of a fourfold superstructure with regard to the perovskite basic cell ($a \approx a_p$ and $c \approx 4a_p$). The variation of the γ value can be followed in Fig. 3. Considering the relative positions of the second order satellites (such as $001\bar{2}$ and 0002) which get closer as x increases, the coalescence of these two reflections is observed for $x = 0.50$.

AVERAGE STRUCTURES

Members $x \leq 0.43$

For the members $x \leq 0.43$, the XRPD patterns do not evidence any extra peak or any subcell distortion. From the ED study, the actual cell of these members is cubic with the space group *Pm3m* for $x = 0.33$ with $a \approx a_p$. *Fm3m* for $x = 0.35$ with $a \approx 2s_p$, and tetragonal with the space group *P4/mmm* for $x > 0.37$ with $a \approx a_p$. This information is not available from XRPD data and the structural refinements were therefore carried out, in a first step, considering the *Pm3m* space group for all these members.

The Rietveld analysis is limited to the determination of the thermal displacement parameters since the atoms are in special positions and the chemical composition determined by EDS and chemical analysis. The results of the Rietveld analysis are given in Table 2, and the experimental and calculated patterns are shown in Fig. 5. These results are however of interest because they introduce the problem encountered as x increases. Indeed, the isotropic thermal parameter of the A site drastically increases for the $x \geq 0.40$ members, compared to those obtained for the members $x < 0.40$.

Two conclusions can be drawn for these "cubic" members. First, the distribution of the cations Ba^{2+}/Bi^{3+} and Fe^{3+}/Bi^{3+} is statistic over the A and B sites, respectively. The ED study indeed established that it is not fully true but the deviations from the ideal *Pm3m* cubic perovskite structure are too weak to be detected by XRPD. The second point is that a sort of "disorder" (high thermal parameters) appears in the A site of the perovskite when the bismuth content of this site increases, whereas the thermal factors of the B site remain low. In fact, as evidenced by ED observations, we known that an incommensurate ordering begins to appear for $x \geq 0.40$, coupled with a tetragonal distortion of the cell. Combining these two informations, we can assume that the increase of the isotropic thermal factors might be the signature of this periodic displacement.

Members $x > 0.43$

For the members $x > 0.43$, the tetragonal distortion is clearly observed by XRPD as well as ED through the presence of extra satellite reflections. But in the present

[2] Tetragonal symmetry is evidences by XRPD only for the terms $x > 0.43$.

TABLE 2
Cell Parameter and Thermal Factors for the Cubic Perovskites (or Classed as Cubic from XRD) $[Ba_{2-3x}Bi_{3x-1}][Fe_{2x}Bi_{1-2x}]O_{2+3x/2}$, $0.33 \leq x \leq 0.43$

Space group: *Pm*3*m* (N°221)

Site B	0.5	0.5	0.5	1*b*
Site A	0	0	0	1*a*
Site O	0.5	0	0.5	3*c*

x	a (Å)	B (Å^2) site A	B (Å^2) site B	B (Å^2) site O	χ^2	R_{Bragg}	%Bi (site *A*–*B*) from nominal x value
0.33	4.0937(1)	0.1(1)	0.3(2)	1.59(9)	2.2	5.5%	0–33
0.35	4.0977(1)	0.8(1)	0.5(2)	0.3(6)	3.5	5.3%	5–30
0.37	4.0819(1)	0.7(2)	0.4(3)	0.4(9)	2.9	6.0%	11–26
0.40	4.0685(1)[a]	2.1(3)	0.5(3)	2(1)	2.8	3.6%	20–20
0.43	4.0515(1)[a]	4.2(3)	1.4(3)	2.4(1.2)	3.1	5.7%	29–14

[a] Satellites in ED patterns shows that the actual symmetry is tetragonal with $\mathbf{q} = \gamma\mathbf{c}^*$.

study, we will only consider the reflections of the basic perovskite subcell. The actual incommensurate structure will be presented in a next paper (11). The occupancies of the two cationic sites are fixed based on the results of the EDS analyses. According to the chemical analyses, which showed that the oxygen content implies the oxidation states Ba^{2+}, Fe^{+3}, and Bi^{+3}, anionic vacancies should exist. They were arbitrarily considered as statistically distributed over the two anionic sites. The Rietveld analysis was performed in the *P*4/*mmm* space group and, once again, only the thermal factors can be refined.

To obtain primary information about the atomic positions which are mostly affected by the periodic deviation, it is interesting to use anisotropic terms to describe the thermal parameters. Despite the carefulness of the XRPD data collection, getting reliable thermal factors from the X-ray diffraction is difficult expecially for light atoms. To this aim we have combined neutron powder diffraction (NPD) and XRPD data, collected on the same samples. In this case, the crystallographic model was refined from the two sets of data simultaneously, using the program XND. The results are given in Fig. 6a and b, for $x = 0.45$ and $x = 0.48$, respectively.

As for the members $x = 0.40$ and $x = 0.43$, the isotropic thermal parameters found for the cations on the A site are very high, increasing as x increases (Table 3). Considering the anisotropic factors, the thermal motion of the A cations appears strongly anisotropic, with the c direction as a privileged direction ($u_{33} > u_{11}$) (see Table 3 and ORTEP representation in Fig. 7). The amplitude of the displacements correlated to the calculated anisotropic thermal parameters is too high to express only the dynamical disorder generated by a thermal vibration. More likely, they indicate that the A cations are displaced along the c axis from their average position. Now, considering the existence of the modulation, this result suggests that the A cations are strongly affected by the periodic deviation but still a static disorder for the A site cannot be ruled out.

To explain these high thermal factors, we can also consider the possibility of the existence of some cationic vacancies on the A site for the members $x > 0.40$. But then, to recover acceptable thermal parameters, the amount of vacancies is incompatible with the chemical composition found for the compounds.

The thermal parameters of the B cations are small and compatible with a disorder generated by the thermal motion. This thermal motion is isotropic for the member $x = 0.45$ and slightly anisotropic for the member $x = 0.48$. This suggests that the B cations (mainly iron) are only weakly affected by the periodic deviation along the c axis.

For the oxygen atoms, abnormally high displacement is observed for the O(2) oxygen position along the c axis, in both, $x = 0.45$ and $x = 0.48$ samples. Once again, this suggests that this oxygen is affected by the periodic deviation. For the O(1) oxygen, the situation is quite different depending on the x value: for $x = 0.45$, the greatest amplitude of displacement is in the (a, b) plane whereas for $x = 0.48$, the amplitude is important within the (a, b) plane as well as along the c axis. The situation of the O(1) oxygen appears more complex with the possible existence of displacements due to the periodic deviation along the c-axis but also probably some static disorder.

These results confirm that these oxides belong to the oxygen deficient perovskite family. They evidence the distribution of Bi(III) over the two sites, A and B simultaneously. However, the actual structure is much more complex, as

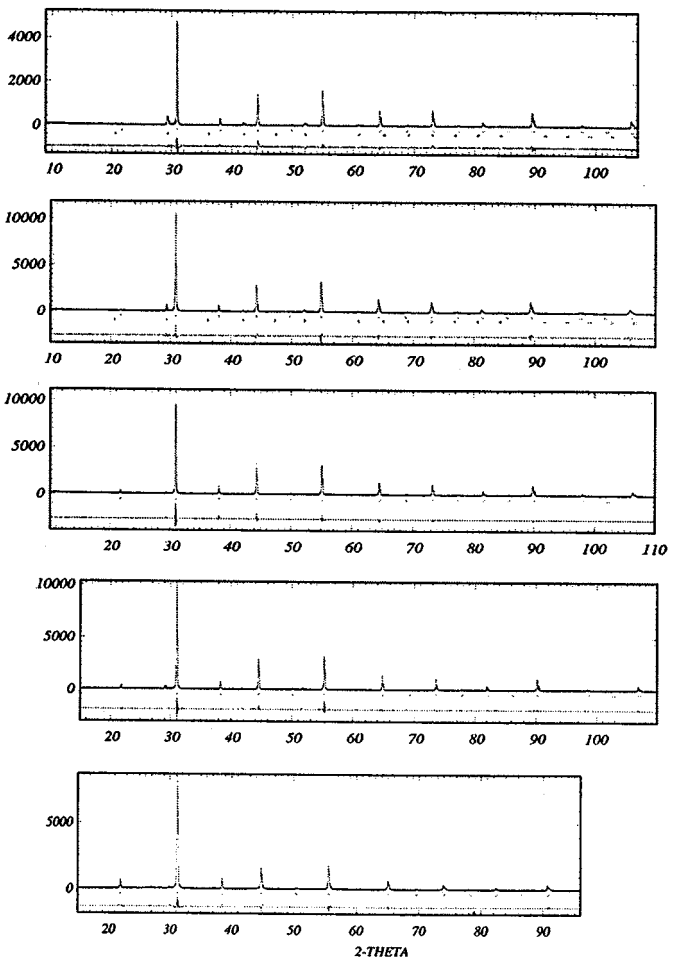

FIG. 5. Experimental and calculated XR diffractograms of the $x = 0.33$, 0.35, 0.37, 0.40, and 0.43 samples. (Top to bottom.)

suggested by the high thermal factors of some atoms and also by the interatomic distance (see Table 4). If the A–O distances are in agreement with the size of Ba^{2+}, ranging from 2.8 to 2.9 Å, they are much higher than expected for Bi^{3+} which should tend to adopt a different coordination due to its $6s^2$ lone pair (13). In a similar way, the B–O distances, ranging from 2.026 to 2.047 Å, although they are in agreement with the size of Fe^{3+}, are slightly too short for Bi^{3+}.

The resolution of the incommensurate structure, which will be the object of the next paper, will allow this question to be answered. In particular it will be shown that the two types of cations sharing the A sites, Bi^{3+} and Ba^{2+}, are not affected by the same displacements with respect to the ideal positions of the tetragonal subcell.

MÖSSBAUER SPECTROSCOPY

The ^{57}Fe Mössbauer spectra of the tetragonal $x = 0.43$, 0.45, 0.48, and 0.50 terms were recorded at 293 K (Fig. 8). The presence of magnetic sextuplets in all the spectra confirms the magnetic behavior observed at this temperature by susceptibility measurements. For the $x = 0.40$ member, the magnetic ordering appears to be not fully established at room temperature, and consequently, the lower $x < 0.43$ members of the series cannot be included in the present study.

The line broadening suggests different local environments for the Fe ions, in agreement with the X-ray and neutron diffraction studies. We have fitted these spectra by two methods, using either an hyperfine field H_f distribution or three independent line widths for each sextuples subspectrum (program MOSFIT (13)). The best fit consists of two iron sites for each composition and was obtained with the latter method (Table 5). The resulting isomer shift, (IS = 0.35–0.41 mm s^{-1} relative to metallic iron), and hyperfine field (H_f = 43–50 T) values are characteristic of the trivalent high spin states for iron. In spite of the lack of Mössbauer spectra in the high temperature paramagnetic domain, one can attempt to estimate the quadrupole splitting QS value. The latter reflects the local environment of the iron site from the following equation: $2\varepsilon = (QS/2)(3\cos^2\theta - 1)$, were 2ε is the quadrupole line shift in the magnetic phase and θ the orientation of H_f with respect to the principal axis of the EFG electric field gradient. In

TABLE 3
X-Ray/Neutron Diffraction Study: Rietveld Analysis of the Average Structure for $x = 0.45$ and 0.48

Space group: $P4/mmm$ (No. 123)				
Site	x	y	z	Wyckoff site
B	0.5	0.5	0.5	1*d*
A	0	0	0	1*a*
O_1	0.5	0.5	0	1*c*
O_2	0.5	0	0.5	2*e*

Site	B_{eq}(Å^2)	u_{11}	u_{33}	Occupancy (from EDS)
$x = 0.45$: $a = 4.0142(2)$ Å and $c = 4.0845(5)$ Å				
A	4.2	0.036(3)	0.089(7)	Ba/Bi: 0.63(2)/0.37(2)
B	1.3	0.016(2)	0.016(4)	Fe/Bi: 0.94(2)/0.06(2)
O_1	2.1	0.33(5)	0.016(7)	0.9
O_2	1.7	0.020(3)	0.027(5)	0.9
X-ray: *Gof* = 2.3, R_{wp} = 11.1%, R_{Bragg} = 12.2%, R_F = 26.2%				
Neutrons: *Gof* = 2.1, R_{wp} = 8.7%, R_{Bragg} = 6.6%, R_F = 4.3%				
$x = 0.48$: $a = 3.9954(7)$ Å and $c = 4.090(1)$ Å				
A	4.7	0.028(3)	0.12(1)	Ba/Bi: 0.57(2)/0.43(2)
B	1.2	0.014(3)	0.019(6)	Fe/Bi: 0..96(2)/0.04(2)
O_1	2.5	0.035(8)	0.03(1)	0.9
O_2	1.9	0.017(4)	0.039(9)	0.9
X-ray: *Gof* = 2.2, R_{wp} = 8.6%, R_{Bragg} = 10.0%, R_F = 14.1%				
Neutrons: *Gof* = 2.2, R_{wp} = 10.2%, R_{Bragg} = 9.2%, R_F = 7%				

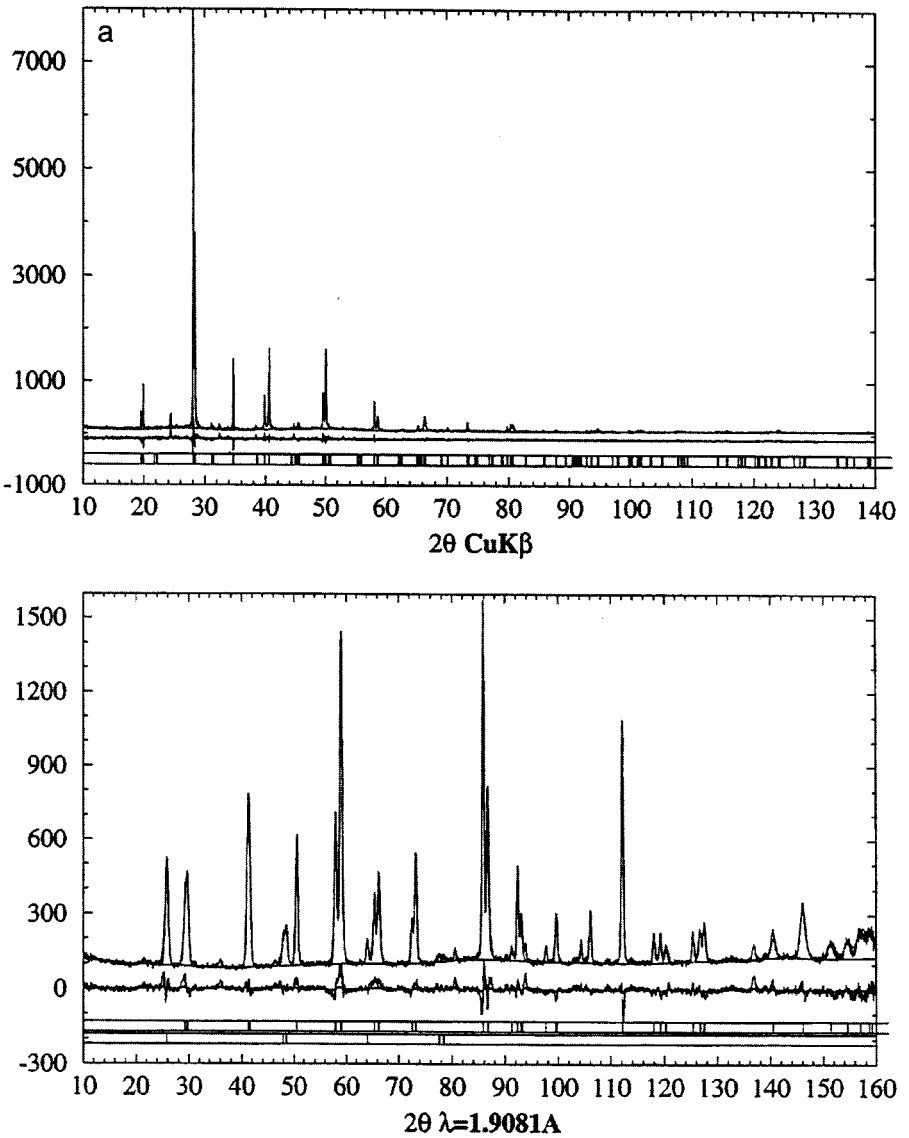

FIG. 6. Results of the Rietveld analysis of the XRD and ND patterns for (a) $x = 0.45$ and (b) $x = 0.48$. The second row of reflections indicated by bars below the ND patterns correspond to the most intense magnetic reflections.

TABLE 4
Evolution of the Interatomic Distances in the Perovskites $[Ba_{2-3x}Bi_{3x-1}][Fe_{2x}Bi_{1-2x}]O_{2+3x/2}$

x	B–O (Å)	A–O (Å)	%Bi (site A–B)
0.33	2.047×6	2.895×12	0–33
0.35	2.049×6	2.898×12	5–33
0.37	2.041×6	2.886×12	11–26
0.40	2.034×6	2.877×12	20–20
0.43	2.026×6	2.865×12	29–14
0.45	2.007×4, 2.042×2	2.864×8, 2.839×4	35–10
0.48	1.998×4, 2.045×2	2.859×8, 2.825×4	44–4
0.50	1.990×4, 2.047×2	2.855×8, 2.814×4	50–0

TABLE 5
Isomer Shift (IS), Quadrupole Shift (2ε), Hyperfine Field (H_f), and Relative Spectral Areas (%) of Subspectra Observed in Room Temperature ^{57}Fe Mössbauer Spectra of $[Ba_{2-3x}Bi_{3x-1}]$ $[Fe_{2x}Bi_{1-2x}]O_{2+3/2x}$

Composition	IS ± 0.02 mm s^{-1}	$2\varepsilon \pm 0.02$ mm s^{-1}	$H_f \pm 0.2$ T	$\pm 5\%$
0.50	0.39	− 0.18	49.8	44
	0.37	− 0.03	46.9	56
0.48	0.41	− 0.15	49.4	46
	0.35	− 0.03	45.7	50
	0.26	0	0	4[a]
0.45	0.40	− 0.14	47.2	49
	0.37	− 0.04	43.2	48
	0.196	0	0	3[a]
0.43	0.35	− 0.01	38.0	64

[a] Nonidentified paramagnetic impurity.

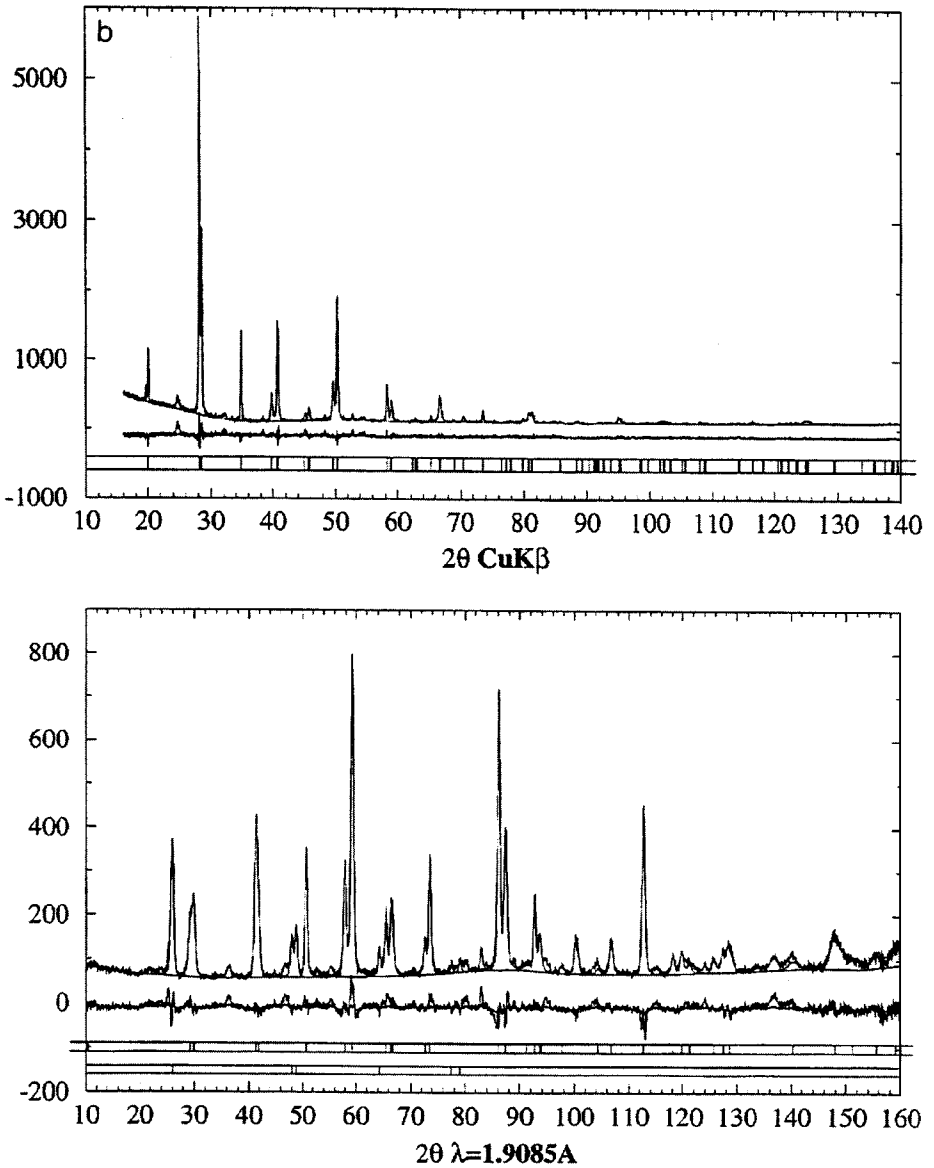

FIGURE 6—*Continued*

a tetragonal structure, one can suppose this principal axis is oriented along the c axis. According to the magnetic structure, refined from neutron diffraction data for the compound $x = 0.5$ (11), the magnetic moment of iron is lying in the (a, b) plane ($\theta = 90°$), so that one can deduce the QS values (0.36 and 0.06 mm s^{-1}) corresponding to $2\varepsilon = 0.18$ and 0.03 mm s^{-1}, respectively, in this compound. The QS lower value 0.06 mm s^{-1}) of the second site is typical of a quasi symmetric environment.

EVIDENCE FOR MAGNETIC TRANSITIONS

Magnetic susceptibility measurements versus temperature, were performed using the Faraday method, in the

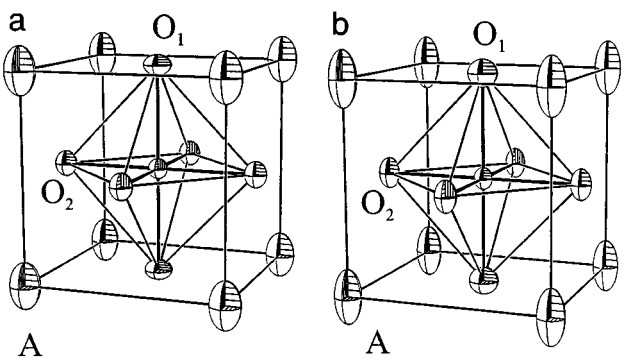

FIG. 7. ORTEP representation of the anisotropic thermal parameters for the compounds (a) $x = 0.45$ and (b) $x = 0.48$.

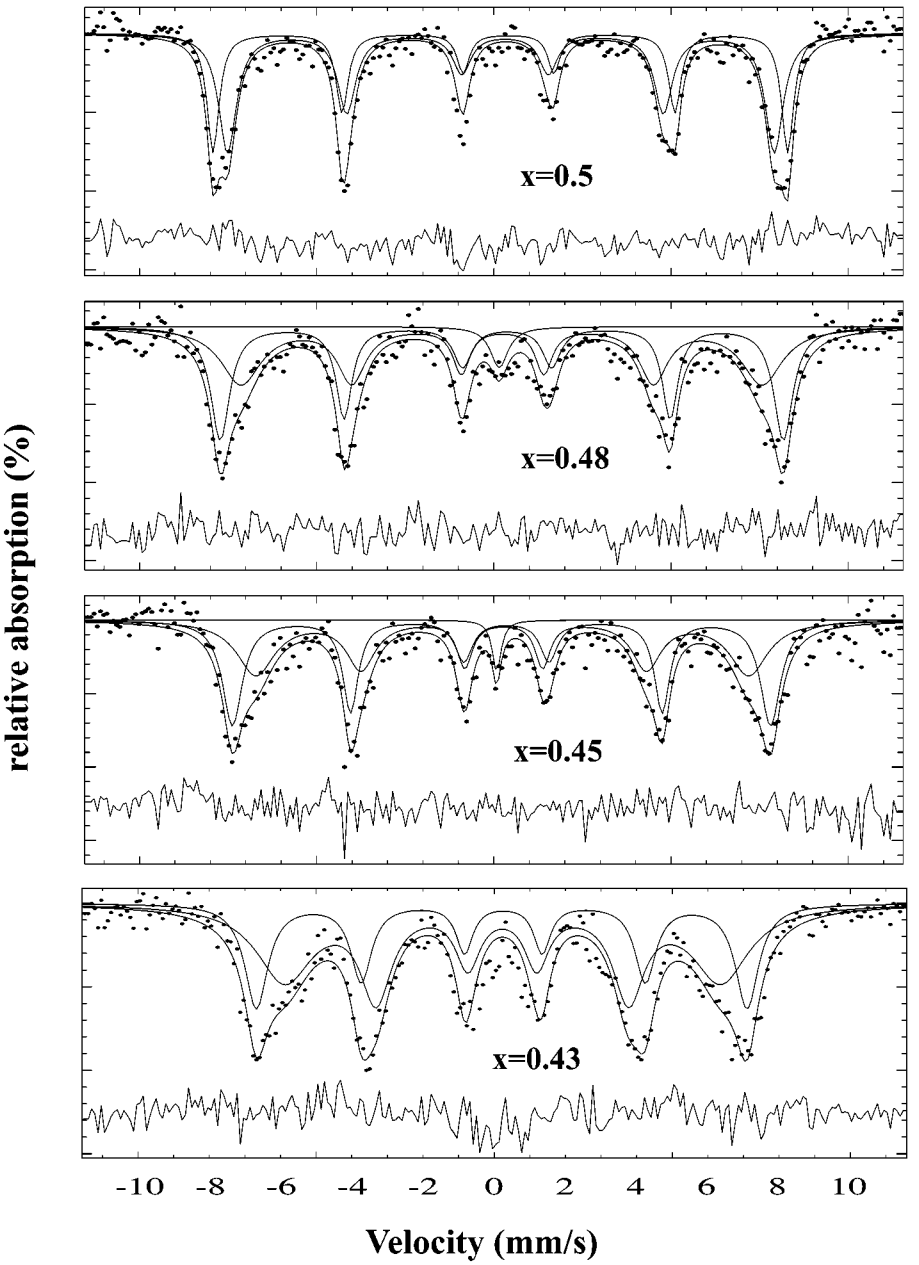

FIG. 8. ^{57}Fe Mössbauer spectra of the $x = 0.43$, 0.45, 0.48, and 0.50 samples (recorded at 293 K).

range 80–900 K, for $x = 0.40$, 0.45, and 0.50. The $\chi(T)$ curves of these samples (Fig. 9a) show that for $x \geq 0.45$, there exists a broad magnetic transition which spreads from 620 to 720 K. The $\chi^{-1}(T)$ curves (Fig. 9b) show that θ_p is very negative, indicating strong antiferromagnetic interactions between Fe^{3+} moments. However, one observes that the magnetic susceptibility increases beyond the transition, as in the case of ferromagnetic materials. The measurement of magnetization versus applied field for $x = 0.50$ at 5 K (Fig. 10) shows that M varies with H and increases in the same way as a ferromagnetic but, the amplitude of the variation is three orders of magnitude smaller. The magnetic moment is indeed of $10^{-3}\ \mu_B$ per iron atom. The neutron diffraction study of this phase, which will be published later (11), shows that the magnetic structure is antiferromagnetic and does not allow any ferromagnetic impurity to be detected. Thus, we can conclude that the existence of such a magnetic moment in an antiferromagnetic structure corresponds to a weak ferromagnetic perovskite (15). The value of the magnetic moment, close to those usually observed for weak

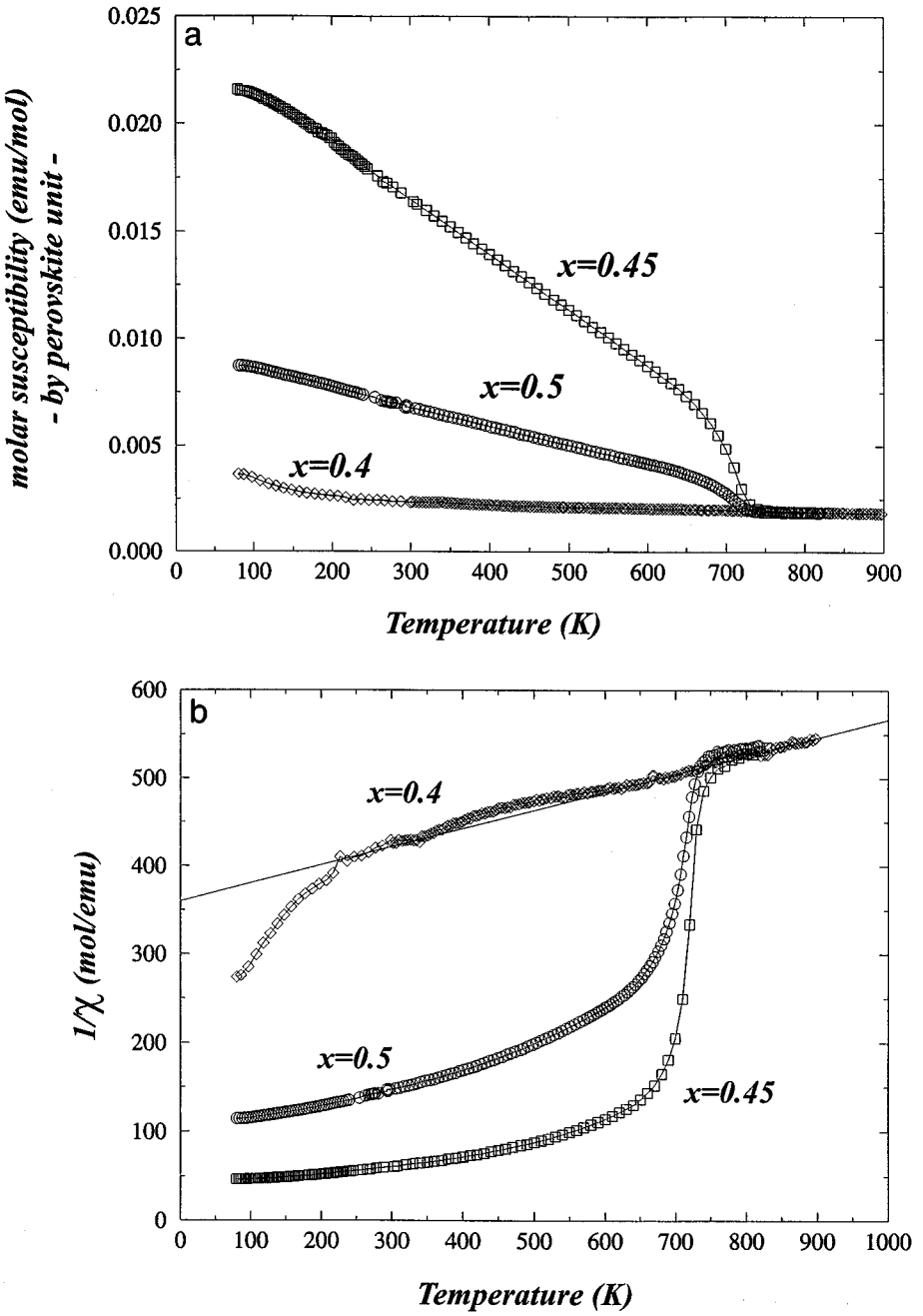

FIG. 9. (a) Magnetic susceptibility versus T in the range 80–900 K. (b) $\chi^{-1}(T)$.

ferromagnetic compounds, supports also this statement. The $\chi^{-1}(T)$ curve of the $x = 0.40$ sample, whose T_N temperature is lower than room temperature (Fig. 9b), allow the spin state of iron to be estimated. The slope of the straight line, modeled according to the Curie–Weiss law, for the paramagnetic domain, of 0.23 leads to a magnetic moment of 5.89 μ_B, i.e. close to the theoretical value for Fe^{3+} in high spin configuration (5.9 μ_B). This result also confirms that iron exhibits exclusively the trivalent state in this compound.

Calorimetric measurements performed with an ATD/DSC facility (SETARAM Labsys), on the $x = 0.50, 0.45$, and 0.40 samples allow also the magnetic transition to be detected. The $q(T)$ curves (Fig. 11) were registered in a nitrogen flow with heating and cooling speeds of $20°.mn^{-1}$. A preheating cycle was carried out before recording. The

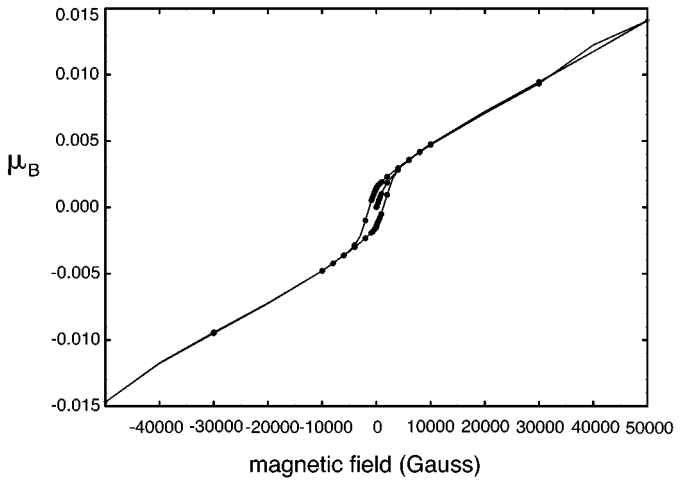

FIG. 10. Magnetization versus applied field for $x = 0.5$.

temperature rising is rapid in order to evidence the magnetic transition. Observe that the transition for $x = 0.50$ appears clearly at 620 K at increasing temperature, which corresponds to the complete ordering of the magnetic structure. The reverse transition is obtained by cooling the sample. Although the actual measurement of the transition temperature is not possible by this method, the decrease of the transition temperature, observed for $x = 0.45$ is significant. Finally it is confirmed that the $x = 0.40$ sample is no more magnetically ordered at room temperature.

CONCLUDING REMARKS

This study of the Ba–Bi–Fe–O system has allowed a new series of perovskites $[Ba_{2-3x}Bi_{3x-1}][Fe_{2x}Bi_{1-2x}]O_{2+3x/2}$ to be isolated, different from the perovskites $[Ba_{1-y}Bi_y][Fe_{1-y}Bi_y]O_{3-y}$ previously isolated by Zanne *et al.* (8). The present series differs from the first one by the total absence of Fe(IV) and Bi(V) in the structure. In the two series, bismuth, is distributed between the two A and B sites and a rather high oxygen deficiency exists. In fact, considering the pseudo ternary diagram "$BiO_{1.5}$–$FeO_{1.5}$–BaO" (Fig. 12), it can be seen that the two series exhibit very different cationic compositions, except for $x = 0.4$, i.e. $[Ba_{0.8}Bi_{0.2}][Fe_{0.8}Bi_{0.2}]O_{2.60}$ which sits at the intersection of the lines "$[Ba_{2-3x}Bi_{3x-1}][Fe_{2x}Bi_{1-2x}]O_{2+3x/2}$" and $[Ba_{1-y}Bi_y][Fe_{1-y}Bi_y]O_{2.5+(1/2)}$, i.e. at $y = 0.2$. The compound $Ba_{0.8}Bi_{0.4}Fe_{0.8}O_{2.648}$ previously synthesized by Zanne *et al.* (8) is indeed very close to our $x = 0.40$ sample, except that if contains some Fe^{4+}; the magnetic moment observed by the authors for this phase, of 4.9 μ_B, smaller than ours (5.98 μ_B), is in agreement with their hypothesis concerning the presence of Fe^{4+} as a low spin cation, Fe^{3+} being in a high spin configuration.

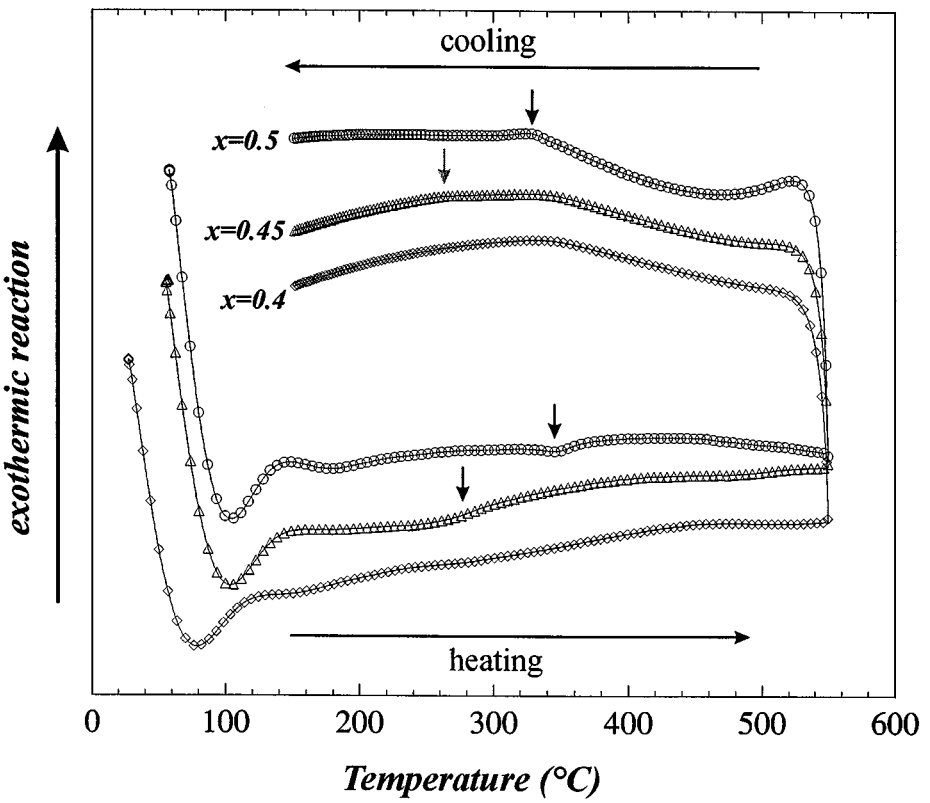

FIG. 11. $q(T)$ registered in flow of N_2.

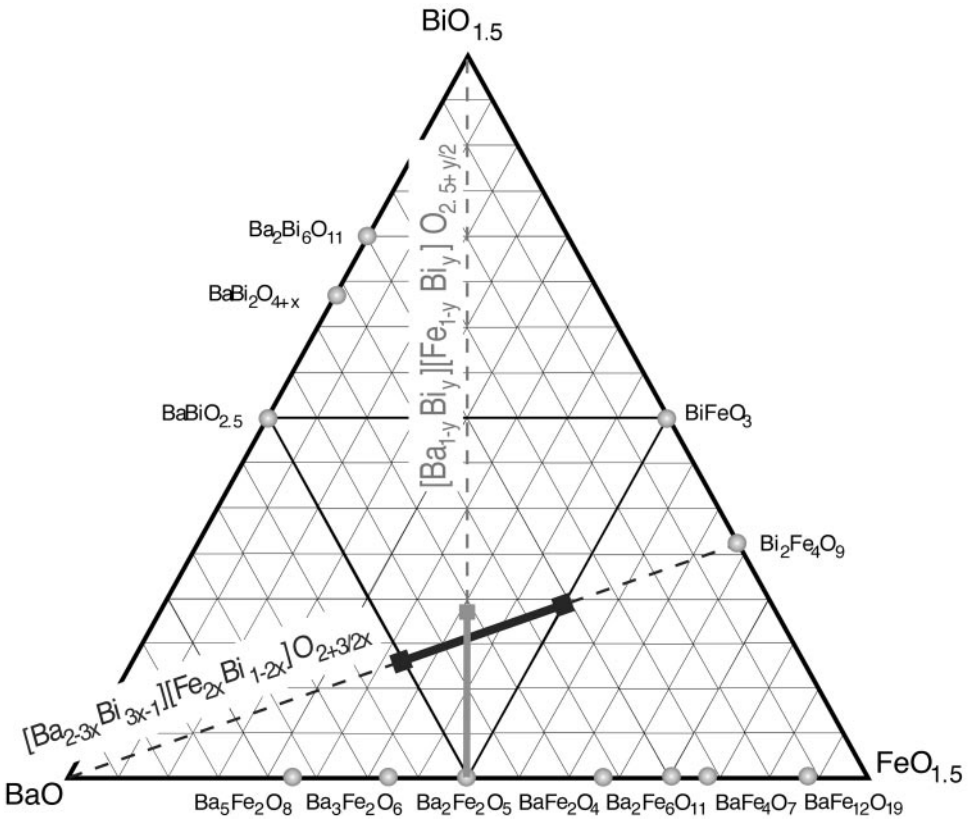

FIG. 12. Pseudo ternary diagram "$BiO_{1.5}$–$FeO_{1.5}$–BaO".

The present perovskites differ also from those described by Zanne *et al.* (4) by the existence of a magnetic transition and the presence of weak ferromagnetism.

The structure of these oxides is in fact very complex, showing incommensurate ordering phenomena, especially for $0.43 \leq x \leq 0.50$, due to the fact that cations as different as Ba^{2+} and Bi^{3+} or Bi^{3+} and Fe^{3+} should occupy the same kind of sites, A and B respectively. Our next paper will shed light on the nuclear and magnetic incommensurate structures of these oxygen deficient perovskites.

ACKNOWLEDGMENTS

The authors thank the CPS Laboratory at the Ecole Centrale of Paris, especiaklly Doctor G. Baldinozzi for data collection, for giving us the possibility to use their prototype diffractometer. They are grateful to Dr. E. Suard (Institut Laüe-Langevin, Grenoble, France) for use of the neutron diffraction facilities.

REFERENCES

1. S. Galasso, "Structure, properties and preparation of perovskite type compound." Pergamon Press, Oxford, 1969.
2. A. W. Sleight, J. L. Gilson, and P. E. Bierstedt, *Solid State Commun.* **17,** 27 (1975).
3. (a) L. F. Mathiess, E. M. Gyorgy, and D. W. Johnson, Jr., *Phys. Rev. B* **37,** 3745 (1988). (b) R. J. Cava, B. Batlogg, J. J. Krajeweski,. R. C. Farrow, L. W. Rupp, Jr., A. E. White, K. T. Peck, Jr., and T. Y. Kometani, *Nature* **332,** 814 (1988). (c) D. G. Hinks, B. Dabrowski, J. D. Jorgensen, A. W. Mitchell, D. R. Richards, S. Pei, and D. Shi, *Nature* **333,** 836 (1988).
4. B. Raveau, C. Michel, M. Hervieu, and D. Groult, "Crystal chemistry of high T_c superconducting copper oxide," Springer Series in Materials Science 15. Springer-Verlag, Berlin, 1991.
5. "Colossal magnetoresistance, charge ordering and related properties of manganese oxides" (C. N. R. Rao and B. Raveau, Eds.), World Scientific, Singapore, 1988.
6. M. T. Anderson, K. B. Greenwood, G. A. Taylor, and K. R. Poeppelmeier, *Prog. Solid State Chem.* **22,** 197 (1993).
7. M. T. Anderson, J. T. Vaughey, and K. R. Poeppelmeier, *Chem. Matter* **5,** 151 (1993).
8. M. Zanne, C. Gleitzer, and J. Aubry, *J. Solid State Chem.* **14,** 160 (1975).
9. J. Rodriguez-Carjaval, "Satellite meeting on powder diffraction," XVth Congress of Int. Union of Crystallography, July 1990.
10. G. Charlot and D. Bézier, "Méthodes d'analyse quantitative Minérale." Masson et C^{ie} Editors.
11. Ph. Boullay, D. Grebille, E. Suard, M. Hervieu, and B. Raveau, in preparation.
12. J. F. Bérar, "Satellite meeting on powder diffraction," XVth Congress of Int. Union of Crystalloraphy, July 1990.
13. N. Jakubowicz, O. Pérez, D. Grebille, and H. Leligny, *J. Solid State Chem.* **139,** 194 (1998).
14. F. Varret and J. Teillet, Université du Maine—France, unpublished program.
15. A. Herpin, "Theorie due magnétisme," Bibliothèque des sciences et techniques nucléaires, 1968.